Hindawi
Journal of Mathematics
Volume 2023, Article ID 3210794, 16 pages
https://doi.org/10.1155/2023/3210794

Research Article

Oblique Flow of Shear Thinning Fluid through an Absorptive Radiative Medium with Hall Effect

S. Rana,[1] K. Mahmud,[2] R. Mehmood,[2] and M. M. Bhatti[3,4]

[1]*Department of Mathematics, Faculty of Basic Sciences, University of Wah, Wah Cantt, Pakistan*
[2]*Department of Mathematics, Faculty of Natural Sciences, HITEC University, Taxila Cantt, Pakistan*
[3]*College of Mathematics and Systems Science, Shandong University of Science & Technology, Qingdao 266590, Shandong, China*
[4]*Material Science, Innovation and Modelling (MaSIM) Research Focus Area, North-West University, Mafikeng Campus, Private Bag X2046, Mmabatho 2735, South Africa*

Correspondence should be addressed to M. M. Bhatti; mmbhatti@sdust.edu.cn

Received 3 February 2023; Revised 8 March 2023; Accepted 5 April 2023; Published 20 April 2023

Academic Editor: Watcharaporn Cholamjiak

The assumption of Hall current and ion slip is extremely crucial in several industrial and manufacturing processes, such as MHD (magneto hydrodynamics) accelerators, preservation coils, transmission lines, electric converters, and heating elements. Keeping this in view, the main aim of this article is to present a computational analysis of MHD ion Hall current with nonlinear thermal radiation on the sloping flow of shear thinning fluid through a porous medium on a stretching sheet that allows fluid suction and injection. The major mathematical modelling of governed problems is converted into a system of nonlinear ODEs (ordinary differential equations) by means of appropriate similarity relations. The influence of all relative physical parameters on velocity and temperature is studied through graphs and discussed in a detailed physical manner. Some beneficial mathematical quantities from the practical engineering and industrial point of view, such as skin friction factor and heat transfer rate at the porous surface, are calculated numerically and presented through graphs. It has been observed that flow may become unstable when M is small and the existence of a magnetic field and a porous ground contributes to a highly rough flow over the stretching surface. Suction is actually a resistive force which results in higher skin friction that is beneficial in controlling flow separation. Temperature of the fluid rises with stronger magnetic field and higher thermal radiation effects. The local heat flux decreases as the magnetic field strength and permeability parameter increase.

1. Introduction

Engineers, scientists, and mathematicians face an enormous challenge while dealing with nonlinear rheology of working fluids. There are number of means through which such types of nonlinearity can be confronted. One of the simplest ways in which viscoelastic fluids have been classified is the methodology given by Rivlin and Ericksen [1]. Noll and Truesdell [2] presented stress tensor as a symmetric tensor with velocity gradient and its derivatives in constitutive equations. In this modern era, researchers like [3] have made a lot of contribution in the field of non-Newtonian fluid flows, due their high-tech implication in industries. It is also noteworthy that these types of fluids exhibit very stimulating mathematical features in their governed flow equations. Oblique stagnation point non-Newtonian fluid flow studies become a more exciting challenge for researchers and investigators due to its wide applications in industries. The fluid flow over a stretched surface is highly significant in so many manufacturing practices. Lok et al. [4] studied time-independent viscid incompressible fluid flow impinging at some arbitrary angles of incidence on a stretching panel. Labropulu et al. [5] developed the study of oblique stagnation-point flow of non-Newtonian fluid towards a stretching surface. Mahapatra et al. [6] analysed a time independent 2D radiative oblique stagnation-point flow with heat transfer characteristics on a shrinking sheet. Sadiq et al. [7] described MHD features of oscillatory oblique

stagnation point flow of micropolar nanofluid. Some more studies developing different physical effects on non-orthogonal stagnation point flows dealing with several non-Newtonian models may be found in [8–10].

The nonlinear radiative electrically conducting fluid flow in manifestation of magnetic field is widely beneficial into electrical control generators, cosmological flows, stellar and lunar power control machinery, planetary automobile re-entry, fissionable production plants, and many other engineering areas. At great operational temperatures, nonlinear thermal radiation becomes more vital and obvious, particularly under nonisothermal conditions. Nonlinear thermal radiation is highly significant when polymer extrusion procedure is monitored by thermally controlled environment. The influence of linear as well as nonlinear thermal radiation on Newtonian as well as non-Newtonian fluid flows in the presence as well as absence of magnetic field has already been discussed by numerous researchers and scientists [11, 12].

Hall and ion currents in influence with magnetic field is the most noteworthy phenomena in modern research due to its intensive, keen-sighted, and immense implications in abundant engineering fields such as power control originators, MHD generators, preservation coils, broadcast ranks, electrical converters, and boiler essentials. By applying Ohm's law directly, mostly the required results are unattainable due to weak magnetic strength but it can be enhanced by adding Hall and ion slip effects in this law. When applied magnetic field is in the direction of magneto hydrodynamics force in combination with Hall ion slip currents, then it becomes tremendously noteworthy in modern research because Hall and ion currents have strong influence on size and track of existing density and subsequently on the magnetic meter.

Ibrahim and Anbessa [13] scrutinized the 3D nanofluid flow of Casson fluid in the presence of applied magnetic field with ion Hall currents and mixed convection over an exponentially stretching surface. Krishna et al. [14] investigated combined effects of Hall and ion slips on MHD spinning stream of ciliary momentum of miniscule bacterium over absorbent intermediate. Rajakumar et al. [15] deliberated the flow of Casson fluid in their research, and they explored the influences of free convection with effects of radiation and viscid indulgence in existence with magnetic fields and Hall ion effects. Kumar and Vishwanath [16] established a scientific arrangement of non-Newtonian fluid flow over a permeable surface with a uniform distribution of magnetic field with Hall current and ion slip effects. Shah et al. [17] defined the flow of micropolar nanofluid in presence of thermally radiative rotating disks for investigation of mass flux and heat flux. Few more related studies on the said topic can be found from the references [18–22].

For continuity of fluid flow, suction/injection is highly recommended, particularly in boundary layer flows. Mainly these types of flows have applications in field of aerodynamics and planetary fields where the use of minimum drag forces is ensured. Suction is used for improvement in efficiency of diffusers. Shojaefard et al. [23] investigated the control flow of fluid on the surface of a subsonic aircraft by using suction/injection. Braslow [24] showed that fuel ingesting and pollution caused by subsonic aircraft as well as price of commercial aircrafts can be reduced to a good extent only with the help of suction/injection.

Stagnation point flows under influence of suction injection have become one of the great interests for modern researchers. Zeeshan and Majeed [25] inspected the characteristics of Jeffery fluid past a stretched plate under influence of attractive dipole with suction/injection. Similarly, El-Arabawy [26] studied the impact of radiative heat transfer with suction and injection on a constant rotating sheet for a micropolar fluid. Chamkha et al. [27] examined the properties of chemical species and heat and mass transmission on a stretched surface in a permeable medium. Pandey and Kumar [28] categorized the viscid dissipation with the presence of suction/injection on MHD flow of a nanofluid in a porous medium. Rundora and Makinde [29] discussed third-grade fluid with assumptions of time- and temperature-dependent variable viscosity findings in presence of suction/injection in a porous station. Similar type of studies may be seen in [30–36].

The all cited works of numerous researchers and scientists depicted that inclined flow of non-Newtonian fluid in existence with a strong magnetic field with ion and Hall currents and nonlinear thermal radiation in porous medium with suction injection influence is highly suitable in many engineering problems and found to be new in this combination, although many researchers in this modern era of research have explored these types of problem but not yet this one. The novelty of governed fluid problem is stated as follows:

(i) A picture of the inclined Casson fluid stagnation point flow on a stretched horizontal plate is captured

(ii) Suction injection phenomenon is taken into consideration, and the horizontal stretched plate is supposed to be permeable.

(iii) The body force on this bioconvective nanofluid flow is the magneto hydrodynamic force with ion slip and Hall currents

(iv) Nonlinear thermal radiation is supposed to be added with convective boundary conditions

The current findings and implications are presented by including graphs of fluid distributions that reveal all new impacts of various parameters. Morevoer, validation of current results with previously existing literature for Newtonian case is provided.

2. Mathematical Scheme

The mathematical model is constructed by using assumptions of two-dimensional, steady oblique flow of MHD Casson fluid along with Hall and ion slip conditions with suction injection and nonlinear thermal radiation. To keep surface stretched, two equal balanced forces are applied in opposite directions along the x–axis, and the origin is

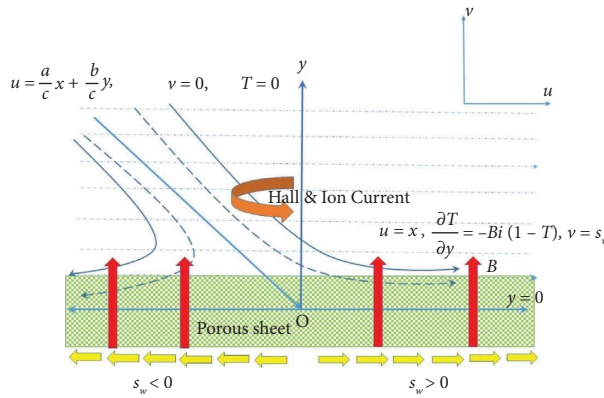

Figure 1: Geometrical description of the governed fluid model.

maintained fixed as shown in Figure 1. The basic fundamental laws in component forms as per stated assumptions are [37–39]

$$\frac{\partial u^*}{\partial x^*} + \frac{\partial v^*}{\partial y^*} = 0, \tag{1}$$

$$u^*\frac{\partial u^*}{\partial x^*} + v^*\frac{\partial u^*}{\partial y^*} + \frac{1}{\rho}\frac{\partial p^*}{\partial x^*} = \nu\left(1 + \frac{1}{\beta}\right)\nabla^{*^2}u^* + \mathbf{J}\times\mathbf{B} - \frac{\upsilon}{K_\alpha}u^*, \tag{2}$$

$$u^*\frac{\partial v^*}{\partial x^*} + v^*\frac{\partial v^*}{\partial y^*} + \frac{1}{\rho}\frac{\partial p^*}{\partial y^*} = \nu\left(1 + \frac{1}{\beta}\right)\nabla^{*^2}v^*, \tag{3}$$

$$u^*\frac{\partial T^*}{\partial x^*} + v^*\frac{\partial T^*}{\partial y^*} = \alpha\left(\frac{\partial^2 T^*}{\partial y^{*^2}} + \frac{\partial^2 T^*}{\partial x^{*^2}}\right) - \frac{1}{\rho c_p}\frac{\partial q_r}{\partial y^*}, \tag{4}$$

$$q_r = -\frac{4\delta^* {T_\infty}^3}{3K^*}\frac{\partial T^{*4}}{\partial y^*}, \tag{5}$$

$$\mathbf{J} = \boldsymbol{\sigma}(\mathbf{E} + \mathbf{V}\times\mathbf{B}) - \frac{\omega_e\tau_e}{\mathbf{B}}(\mathbf{J}\times\mathbf{B}) + \frac{\omega_e\tau_e}{\mathbf{B}^2}\beta_i(\mathbf{J}\times\mathbf{B})\times(\mathbf{B}). \tag{6}$$

The consistent boundary conditions are [39]

$$\begin{aligned} u^* &= cx^*, \\ v^* &= u_f, \\ -k\frac{\partial T^*}{\partial y^*} &= h_s\left(T_f - T^*\right), \\ y^* &= 0, \end{aligned} \tag{7}$$

$$\begin{aligned} u^* &= ax^* + by^*, \\ v^* &= 0, \\ T^* &= T_\infty, y^* \longrightarrow \infty, \end{aligned} \tag{8}$$

where u^* and v^* are the velocity components in x and y directions, and ν, p^*, ρ, T^*, q_r, c_p, T_∞, k^*, c, a, b, and $\beta = \mu_B(\sqrt{2\pi_c}/p_y)$ are the kinematic viscosity, pressure, density, temperature, nonlinear radiative heat flux, specific heat, ambient fluid temperature, thermal coefficient, the constants, and Casson fluid parameter, respectively. $\mathbf{J}\times\mathbf{B}$ is defined as generalised Ohm's law, where $\mathbf{J}$, σ, and $\mathbf{E}$ are the current density, electrical conductivity, and electric field intensity, respectively. Equations (1)–(8) are transformed into nondimensional form [37–39]:

$$\frac{\partial u}{\partial x} + \frac{\partial v}{\partial y} = 0, \tag{9}$$

$$u\frac{\partial u}{\partial x} + v\frac{\partial u}{\partial y} = -\frac{\partial p}{\partial x} + \left(1 + \frac{1}{\beta}\right)\nabla^2 u - \frac{M\left(1 + \beta_i\beta_e\right)}{\left[\beta_e^2 + \left(1 + \beta_i\beta_e\right)^2\right]}u - \Omega u, \tag{10}$$

$$u\frac{\partial v}{\partial x}+v\frac{\partial v}{\partial y}=-\frac{\partial p}{\partial y}+\left(1+\frac{1}{\beta}\right)\nabla^2 v, \tag{11}$$

$$\left(u\frac{\partial T}{\partial x}+v\frac{\partial T}{\partial y}\right)\mathrm{Pr}=\left(\frac{\partial^2 T}{\partial y^2}+\frac{\partial^2 T}{\partial x^2}\right)+Rd\frac{\partial}{\partial y}\left(\left(T\left(\theta_w-1\right)+1\right)^3\frac{\partial T}{\partial y}\right), \tag{12}$$

$$\begin{aligned} u&=x,\\ \frac{\partial T}{\partial y}&=-Bi\left(1-T\right),\\ v&=s_w,\\ \text{at } y&=0, \end{aligned} \tag{13}$$

$$\begin{aligned} u&=\frac{a}{c}x+\frac{b}{c}y,\\ v&=0,\\ T&=0,\\ \text{at } y&\longrightarrow\infty, \end{aligned} \tag{14}$$

where β_e, β_i, Pr, s_w, θ_w, Bi, $M\Omega$, (a/b), and (b/c) represent the Hall parameter, ion parameter, Prandtl number, suction ($s_w>0$)/injection ($s_w<0$) parameter, temperature ratio parameter, Biot number, magnetic field parameter, permeability parameter, stretching ratio parameter, and obliqueness of the flow, respectively.

By stream-function transformation as defined [38] in equations (9)–(14) with $p_{xy}=p_{yx}$,

$$\frac{\partial\psi}{\partial y}\left(\frac{\partial^3\psi}{\partial x^3}+\frac{\partial^3\psi}{\partial y^2\partial x}\right)-\frac{\partial\psi}{\partial x}\left(\frac{\partial^3\psi}{\partial y^3}+\frac{\partial^3\psi}{\partial x^2\partial y}\right)-\left(1+\frac{1}{\beta}\right)\nabla^4\psi+\frac{M\left(1+\beta_i\beta_e\right)}{\left[\beta_e^2+\left(1+\beta_i\beta_e\right)^2\right]}\frac{\partial^2\psi}{\partial y^2}+\Omega\frac{\partial^2\psi}{\partial y^2}, \tag{15}$$

$$\mathrm{Pr}\left(\frac{\partial\psi}{\partial y}\frac{\partial T}{\partial x}-\frac{\partial\psi}{\partial x}\frac{\partial T}{\partial y}\right)=\left(\frac{\partial^2 T}{\partial x^2}+\frac{\partial^2 T}{\partial y^2}\right)+Rd\frac{\partial}{\partial y}\left(\left(T\left(\theta_w-1\right)+1\right)^3\frac{\partial T}{\partial y}\right), \tag{16}$$

$$\begin{aligned} \frac{\partial\psi}{\partial y}&=x,\\ -\frac{\partial\psi}{\partial x}&=s_w,\\ \frac{\partial T}{\partial y}&=-Bi\left(1-T\right),\\ y&=0, \end{aligned} \tag{17}$$

$$\begin{aligned} \frac{\partial\psi}{\partial y}&=\frac{a}{c}x+\frac{b}{c}y,\\ T&=0,\\ \text{at } y&\longrightarrow\infty. \end{aligned} \tag{18}$$

Over consuming stream-function transformation as defined in [38] into equations (15)–(18) and after integration once,

$$\left(1+\frac{1}{\beta}\right)f'''+ff''-\left(f'\right)^2-\frac{M\left(1+\beta_i\beta_e\right)}{\beta_e^2+\left(1+\beta_i\beta_e\right)^2}f'-\Omega f'+B_1=0, \tag{19}$$

$$\left(1+\frac{1}{\beta}\right)g'''+fg''-f'g'+\frac{M\left(1+\beta_i\beta_e\right)}{\beta_e^2+\left(1+\beta_i\beta_e\right)^2}g'-\Omega g'+B_2=0, \tag{20}$$

$$\theta'' + \Pr\ f\theta' + Rd\left(\left(\theta(\theta_w - 1) + 1\right)^3\theta'\right)' = 0. \tag{21}$$

The consistent boundary conditions (17) and (18) convert

$$\begin{aligned} f &= -s_w, \\ f' &= 1, \\ g' &= 0, \\ \theta' &= -Bi\,(1 - \theta(0)), \\ \text{at } y &= 0, \\ f' &= \frac{a}{c}, \\ g' &= \frac{b}{c}y, \\ \theta &= 0, \\ \text{at } y &\longrightarrow \infty, \end{aligned} \tag{22}$$

where B_1 and B_2 can be obtained from B.Cs (23) as

$$\begin{aligned} B_1 &= -\frac{a}{c}\left(\frac{M\left(1 + \beta_i\beta_e\right)}{\beta_e^2 + \left(1 + \beta_i\beta_e\right)^2} + \frac{a}{c} + \Omega\right), \\ B_2 &= \frac{b}{c}\left(A - \frac{M\left(1 + \beta_i\beta_e\right)}{\beta_e^2 + \left(1 + \beta_i\beta_e\right)^2}y - \Omega y\right). \end{aligned} \tag{24}$$

Defining the transformation

$$g'(y) = \gamma_2 h(y), \tag{25}$$

we get

$$\left(1 + \frac{1}{\beta}\right)f''' + ff'' - \left(f'\right)^2 - \frac{M\left(1 + \beta_i\beta_e\right)}{\beta_e^2 + \left(1 + \beta_i\beta_e\right)^2}f' + \frac{a}{c}\left(\frac{M\left(1 + \beta_i\beta_e\right)}{\beta_e^2 + \left(1 + \beta_i\beta_e\right)^2} + \frac{a}{c} + \Omega\right) = 0, \tag{26}$$

$$\left(1 + \frac{1}{\beta}\right)h'' + fh' - f'h - \frac{M\left(1 + \beta_i\beta_e\right)}{\beta_e^2 + \left(1 + \beta_i\beta_e\right)^2}(h - y) - \Omega(\mathrm{h} - \mathrm{y}) - A = 0, \tag{27}$$

$$\theta'' + \Pr\ f\theta' + Rd\left(\left(\theta(\theta_w - 1) + 1\right)^3\theta'\right)' = 0, \tag{28}$$

$$\begin{aligned} f &= -s_w \\ f' &= 1, \\ h &= 0, \\ \theta' &= -\mathrm{Bi}\,(1 - \theta(0)), \\ \text{at } y &= 0, \end{aligned} \tag{29}$$

$$\begin{aligned} f' &= \frac{a}{c}, \\ h' &= 1, \\ \theta &= 0, \\ \text{at } y &\longrightarrow \infty. \end{aligned} \tag{30}$$

3. Physical Quantities of Interest

Skin friction coefficients at surface and the local heat flux [37] are the physical quantities of interest that have extensive use in numerous engineering and manufacturing productions.

$$\tau_w = \left(1 + \frac{1}{\beta}\right)\left[x f''(0) + \frac{b}{c} h''(0)\right], \qquad q_w = -\theta'(0). \tag{31}$$

The stagnation points x_s are

$$x_s = \frac{-(b/c)h'(0)}{f''(0)}. \tag{32}$$

4. Numerical Scheme

The mathematical form of governed problems (26)–(30) is the system of coupled highly nonlinear set of ordinary differential equations. To solve such system of equations by shooting technique, first of all, make them into set of first-order initial value problem by using following transformation.

$$\begin{pmatrix} f \\ f' \\ f'' \\ f''' \end{pmatrix} = \begin{pmatrix} y_1 \\ y_1' = y_2 \\ y_2' = y_3 \\ y_3' = y_4 \end{pmatrix}, \quad \begin{pmatrix} h \\ h' \\ h'' \end{pmatrix} = \begin{pmatrix} y_5 \\ y_5' = y_6 \\ y_6' = y_7 \end{pmatrix}, \quad \begin{pmatrix} \theta \\ \theta' \\ \theta'' \end{pmatrix} = \begin{pmatrix} y_8 \\ y_8' = y_9 \\ y_9' = y_{10} \end{pmatrix}. \tag{33}$$

We get

$$\left(1 + \frac{1}{\beta}\right) y'_3 = -y_1 y_3 + y_2^2 + \frac{M\left(1 + \beta_i \beta_e\right)}{\beta_e^2 + \left(1 + \beta_i \beta_e\right)^2} y_2 - \frac{a}{c}\left(\frac{M\left(1 + \beta_i \beta_e\right)}{\beta_e^2 + \left(1 + \beta_i \beta_e\right)^2} + \frac{a}{c} + \Omega\right),$$

$$\left(1 + \frac{1}{\beta}\right) y_6' = y_2 y_6 - y_1 y_6 + \left(\frac{M\left(1 + \beta_i \beta_e\right)}{\beta_e^2 + \left(1 + \beta_i \beta_e\right)^2} + \Omega\right)\left(y_5 - y\right) + A,$$

$$y_9' = -\mathrm{Pr} y_1 y_9 + Rd\left\{\left(y_8\left(\theta_w - 1\right) + 1\right)^3 y_9\right\}', \tag{34}$$

$$\left.\begin{aligned} &y_1(0) = \alpha_1, y_2(0) = 1, \\ &y_3(0) = \alpha_2, y_5(0) = 0, \\ &y_6(0) = \alpha_3, y_8(0) = 0, \\ &y_9(0) = \alpha_4, \end{aligned}\right\},$$

where $\alpha_i, i = 1 \ldots 4$, are the shooting factors with assumption of three decimal places tolerance level.

5. Results and Physical Discussion

Comprehensive computational calculations have been conducted and demonstrated by graphs herein segment. The numerical investigation of oblique stagnation point flow of MHD ion Hall current with suction injection of non-Newtonian fluid along with nonlinear thermal radiation in porous medium is presented in this segment. Figures 2–10 are settled to attain the norms and standards of this theoretical research.

Figure 2 is constructed to note the influence of permeability constraint Ω on fluid's normal and tangential velocity $f'(y)$, $h'(y)$, and temperature $\theta(y)$ of fluid with suction/injection. Figure 2(a) presents normal velocity $f'(y)$ shrinkages for rising values of permeability parameter $\Omega = 0.1, 3.0, 5.0, 7.0$, and it is quite evident that the existence of permeable surface becomes the reason of strong restriction to flowing of fluid, so the velocity becomes decelerate. Also, it is worth mentioning here that the magnitude of suction $(s_w > 0)$ is greater than the magnitude of injection $(s_w < 0)$ for this case, higher suction becomes more effective in porous surface as it delays the boundary layer separation and flow becomes more and more stable. Figure 2(b) indicates other component of velocity $h'(y)$ upswings nearby surface since a high permeability allows fluids to pass through more freely, and after inflection point, it reverses its behaviour and comes to decline far off from sheet because of higher inspiration of porousness parameter $\Omega = 0.1, 3.0, 5.0, 7.0$ and behaves extremely resistive. It is noted in this graph that close to wall injection $(s_w < 0)$ is higher than suction but away from the wall effect of suction/

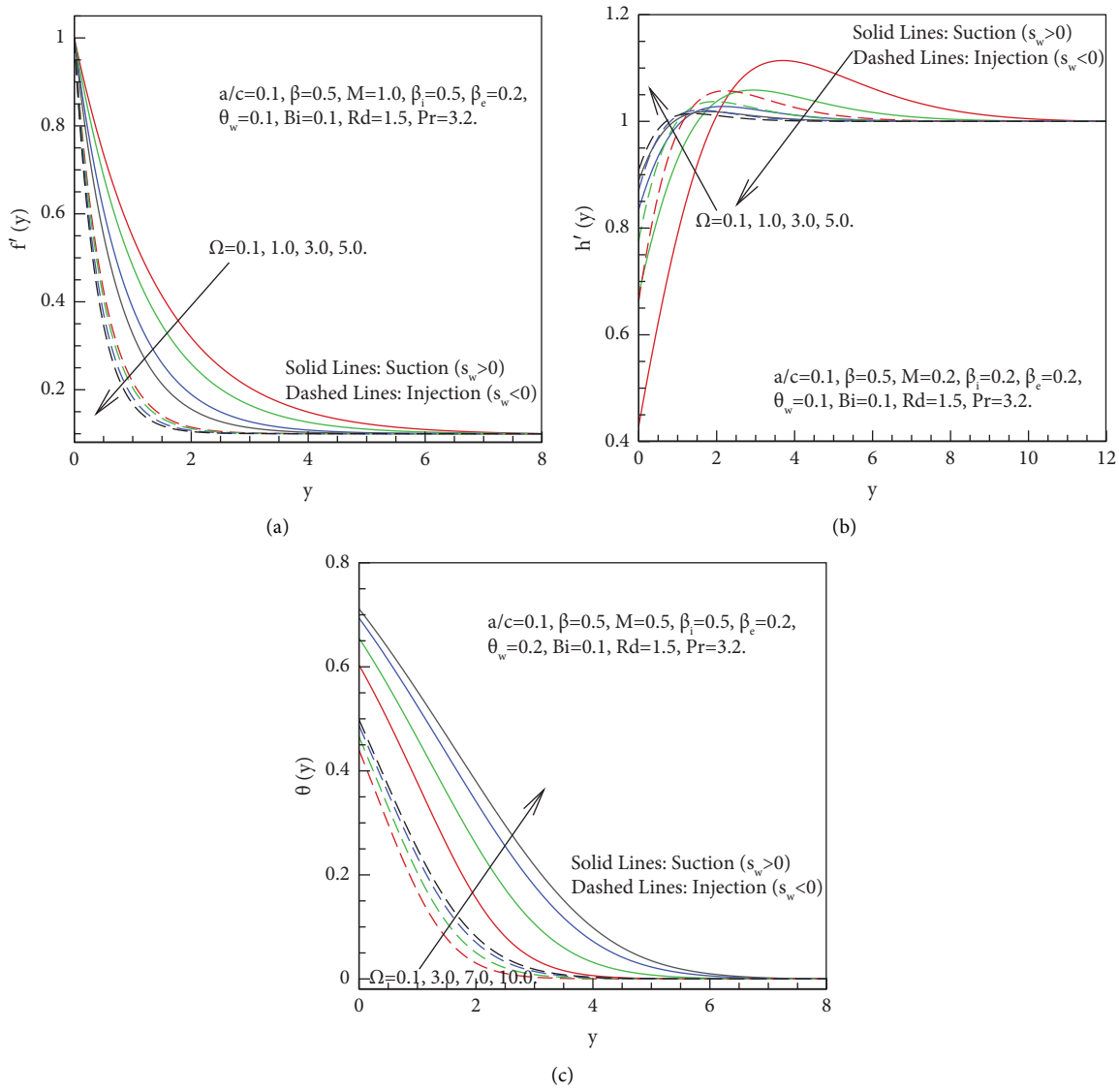

FIGURE 2: (a) Velocity distribution $f'(y)$, (b) velocity distribution $h'(y)$, and (c) temperature distribution $\theta(y)$ for permeability parameter Ω.

injection reversed. Figure 2(c) describes the effect of permeability parameter $\Omega = 0.1, 3.0, 7.0, 10.0$ on temperature of fluid, when permeability parameter Ω rises so that the temperature distribution with thermal boundary layer increases. This happens because permeable surface slows down the motion of fluid flow, and this restriction in flowing of fluid becomes responsible to enhance the temperature of governed fluid. Figure 2(c) also depicts the stronger influence of suction $(s_w > 0)$.

Figure 3 describes the impact of ion slip constraint β_i on fluid's velocities $f'(y)$ and $h'(y)$ as well as on temperature $\theta(y)$ of fluid with suction/injection. Conductivity of fluid increases when values of ion slip constraint $\beta_i = 0.1, 3.0, 6.0, 10.0$ escalates and as a reaction, restraining energy comes down and fluid's molecules freely moves and fluid's velocity raises as noted in Figure 3(a). Figure 3(b) is plotted to show similar kind of increasing behaviour for $\beta_i = 0.1, 2.0, 4.0, 6.0$ away from the surface but at surface velocity reverses its behaviour and declines at wall because at wall fluids have resistance which opposes the flow. Figure 3(c) displays that temperature $\theta(y)$ of fluid declines; also, the thermal boundary layer becomes thinner for ion slip parameter $\beta_i = 0.1, 2.0, 5.0, 8.0$, due to dropping of damping energy in the direction of flow. It is worth mentioning here that velocity profile for suction $(s_w > 0)$ is greater than injection $(s_w < 0)$. Strong influence of suction is highly useful to reduce the drag in boundary layer flow.

Figure 4 is planned to recognize the enactment of both velocities $f'(y)$, $h'(y)$, and temperature $\theta(y)$ of fluid for Hall parameter β_e. Since the resistance is produced by magnetic field when Lorentz force is strong enough, but due to the presence of Hall parameter β_e, the resistive force becomes weak due to decline in conductivity, so fluid's normal velocity $f'(y)$ proliferates with the rise in Hall parameter $\beta_e = 0.1, 0.3, 0.6, 1.0$. as mentioned in 4(a), and for suction $(s_w > 0)$, velocity is greater, but for injection

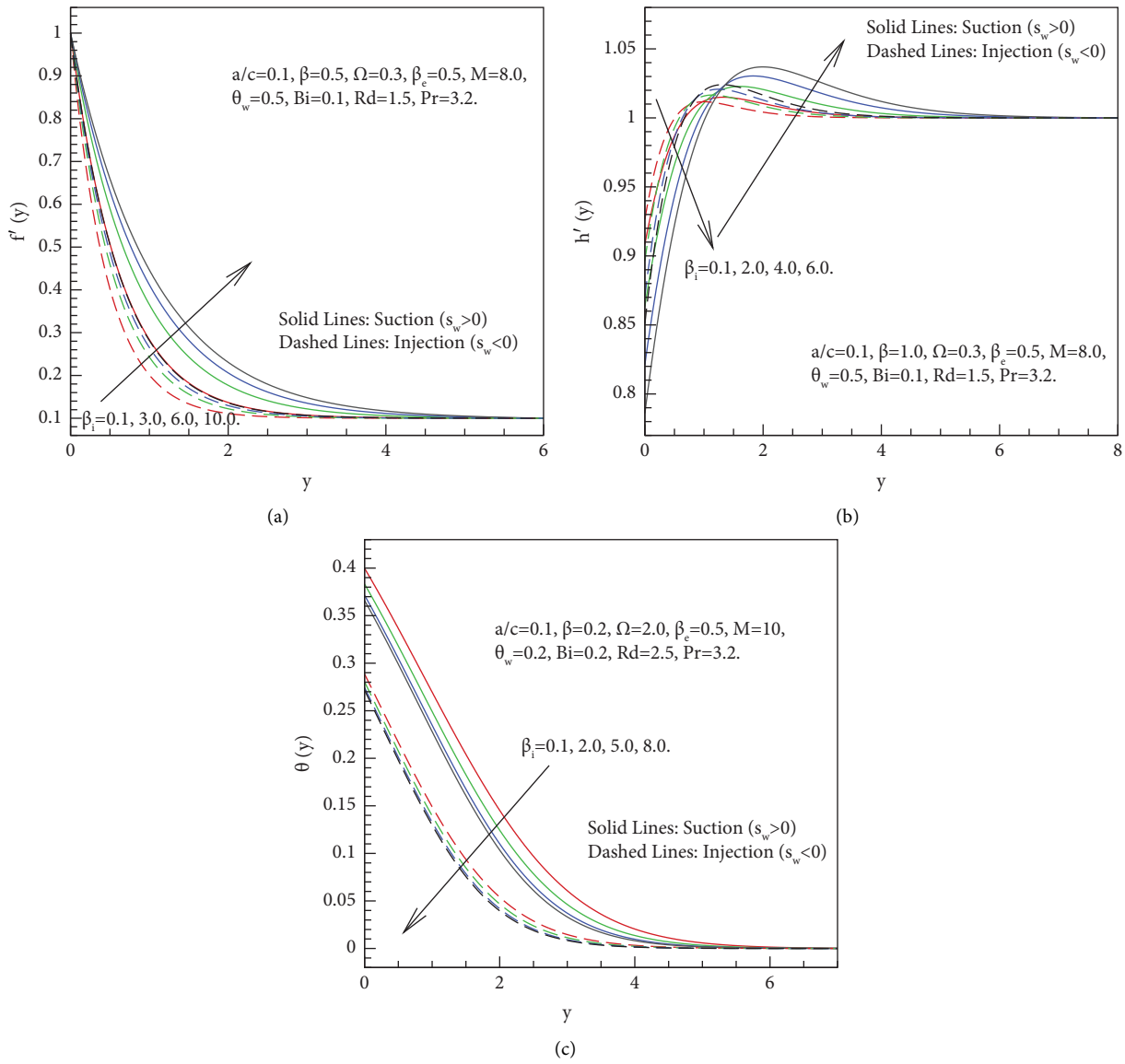

Figure 3: (a) Velocity distribution $f^{'}(y)$, (b) velocity distribution $h^{'}(y)$, and (c) temperature distribution $\theta(y)$ for ion slip parameter β_i.

$(s_w < 0)$, velocity of fluid is smaller. Figure 4(b) expresses the significance of Hall constraint $\beta_e = 0.1, 0.3, 0.6, 1.0$, and it governs when fluid is far away from surface and fluid's tangent component of velocity, $h^{'}(y)$ intensificates away from wall, but near to surface, it takes differing conduct and contracts. Given that the Hall parameter is calculated as the sum of the frequency and the time of electron collisions. An increase in this parameter indicates an increase in the frequency of electrons, the duration of electron collisions, or both. Figure 4(c) shows that temperature $\theta(y)$ drops down when Hall parameter $\beta_e = 0.1, 1.0, 2.0, 5.0$ increases; because of weak resistive force, there is decline in thermal conductivity and as a result the temperature profile declined. The effect of suction $(s_w > 0)$ is stronger in these graphs, and it is more applicable in practical world problems/models and useful for situation where to increase output of diffusers of governed fluid through reducing separation drag. Boundary layer suction particular in porous media close to trailing edge is useful to maximize the lift and minimize the drag force of automobiles, aerofoils, and jet planes.

Figure 5 is intended to show the effect of magnetic field on fluid's velocity and fluid's temperature, every time. The existence of magnetic field means that there is birth of Lorentz strength. Lorentz force is defined as a resistive drag force, so normal velocity $f^{'}(y)$ of fluid descents for $M = 0.1, 1.0, 3.0, 6.0$ as seen in Figure 5(a). But for tangential velocity, $h^{'}(y)$ case is opposite and grows up close to surface but reverses its behaviour when it moves away from the surface for $M = 0.1, 1.0, 3.0, 6.0$, see Figure 5(b). This happens due to the presence of magnetic field. Figure 5(c) contrives to implement the connection of temperature with magnetic field. It shows that temperature $\theta(y)$ increases for higher values of magnetic field $M = 0.1, 3.0, 7.0, 10.0$ because of frictional stress which arise because of Lorentz force, so there occurs increment in thermal conductivity, so in temperature of fluid.

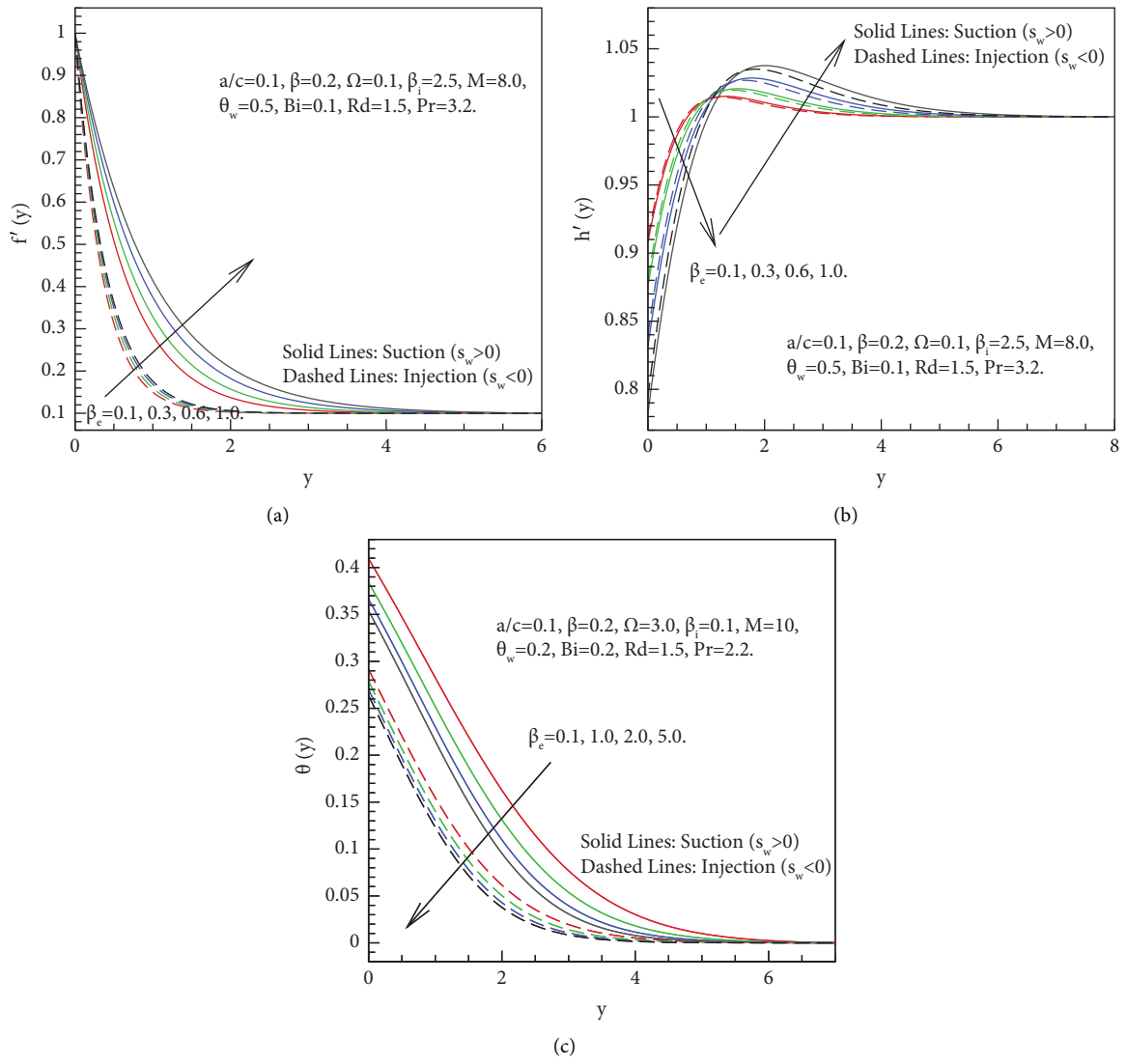

FIGURE 4: (a) Velocity distribution $f'(y)$, (b) velocity distribution $h'(y)$, and (c) temperature distribution $\theta(y)$ for Hall parameter β_e.

Figure 6 is plotted for inspecting the performance of radiation parameter Rd, Biot number Bi, and Prandtl number Pr on temperature distribution. Fluid's temperature $\theta(y)$ enlarged for rising numbers of radiation parameter $Rd = 0.1, 0.5, 1.0, 1.5$ because larger radiation parameter implies more heat is provided to the fluid, so thermal boundary layer becomes thick and temperature of fluid rises as illustrated in Figure 6(a). In addition to being utilised to produce power, radiation is also used in academia, industry, and medical. Radiation is also useful in many other fields, including mining, law enforcement, space exploration, agriculture, archaeology (carbon dating), and many others. Figure 6(b) shows that temperature of fluid becomes higher with growth in Biot number $Bi = 1.0, 1.5, 2.0, 3.0$. Because when convective heat conversation at the surface rises ($Bi \geq 1.0$), then there is enhancement in thermal boundary layer thickness as with a higher heat transfer coefficient, and more heat is transferred from the surface to the fluid. The rate of heat transmission increases with greater estimates of Bi. Bi can, therefore, be used as a cooling operator in complex operations. Figure 6(c) shows the thermal boundary layer thicknesses shrinkage extremely when there is rise in Prandtl number $\mathrm{Pr} = 1.0, 1.5, 2.0, 3.0$; so, there is escalation in the wall temperature gradient. This phenomenon occurs because of higher values Prandtl number, and then, fluid has moderately little thermal conductivity that lessens the occurrence of conduction and reduces the thickness of thermal boundary layer; hence, temperature of fluid declines. Small Prandtl values are a suitable choice for heat-transmitting liquids since they are free-flowing liquids with strong thermal conductivity. Prandtl number ($\mathrm{Pr} < 1.0$) specifies fluids with huge thermal conductivity which crops denser thermal boundary layer as compared to the thermal boundary layer for higher Prandtl number ($\mathrm{Pr} > 1.0$). Suction is more prominent than injection in all these plots, and it is an efficient source for laminar boundary layer flow, it reduces the contact losses at surface and suction becomes

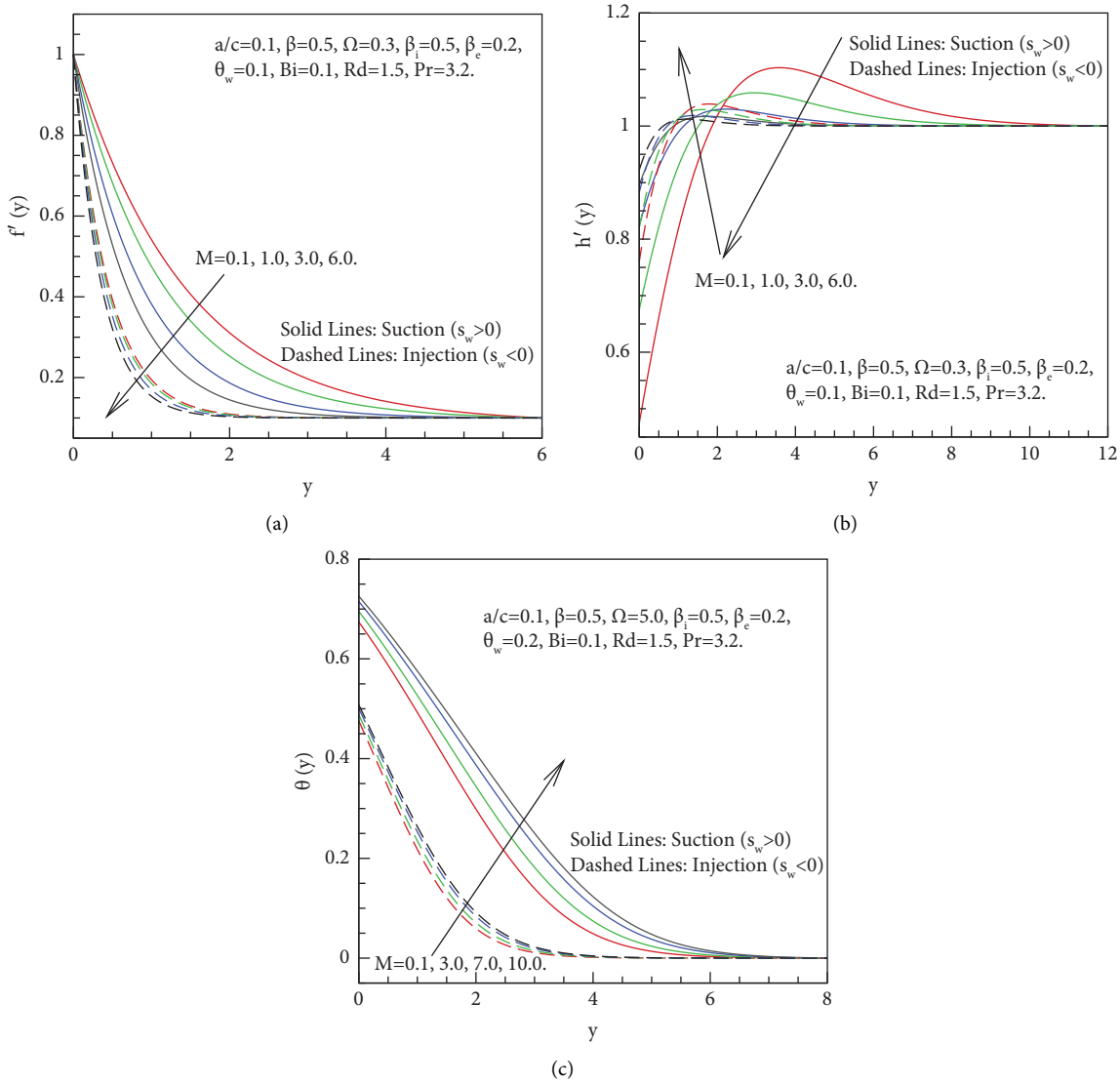

FIGURE 5: (a) Velocity distribution $f^{'}(y)$, (b) velocity distribution $h^{'}(y)$, and (c) temperature distribution $\theta(y)$ for magnetic field parameter M.

more stable in laminar boundary layer, and it becomes thin and remains laminar throughout. These physical quantities are of great worth due to its large and high scales applications in many industrial and engineering arenas, specifically areas of aerodynamics and astronomical, and highly beneficial in controlling flow separation.

Figure 7(a) launches that skin friction coefficient at surface $h^{'}(0)$ increases when permeability parameter $\Omega = 0.1, 0.3, 0.7$ rises with suction $(s_w > 0)$ and injection $(s_w < 0)$, and also, it upsurges when the values of magnetic field M raised for both cases. It is worth noting in this plot that suction is smaller than injection. Figure 7(b) develops the decreasing influence of local heat transfer rate $-\theta^{'}(0)$ rises for permeability parameter $\Omega = 0.1, 0.3, 0.7$ and for magnetic field parameter M for both cases of suction $(s_w > 0)$ as well as for injection $(s_w < 0)$. Also, suction $(s_w > 0)$ is smaller than injection $(s_w < 0)$.

Figure 8(a) indicates skin friction coefficient at wall $h^{'}(0)$ shrinkages when both Hall parameter $\beta_e = 0.1, 0.5, 1.0$ and ion slip parameter β_i increase. Figure 8(b) displays that local heat flux $-\theta^{'}(0)$ grows up for increasing values of Hall parameter $\beta_e = 0.1, 0.5, 1.0$; on the other hand, it remained fixed for ion slip parameter β_i on local heat flux for both cases of suction as well as for injection but influence of suction is smaller than injection in these two plots.

In Figure 9, it is found that effect of radiation parameter $Rd = 0.1, 0.3, 0.7$ is downward for heat transfer rate at surface $-\theta^{'}(0)$ but have opposite behaviour for Biot number Bi. Also, this figure exhibits that injection is stronger and enhancing than suction. The fluid flow in the channel is controlled by suction or injection phenomenon. Figure 10 shows flow pattern through stream lines for suction $(s_w > 0)$ and injection $(s_w < 0)$ in the presence and absence of permeability parameter Ω. Figure 10(a) reveals the flow pattern with and without permeability for injection $(s_w < 0)$ and for suction $(s_w > 0)$ in Figure 10(b). Figure 10(c) simultaneously shows the stream lines pattern for both suction $(s_w > 0)$ as

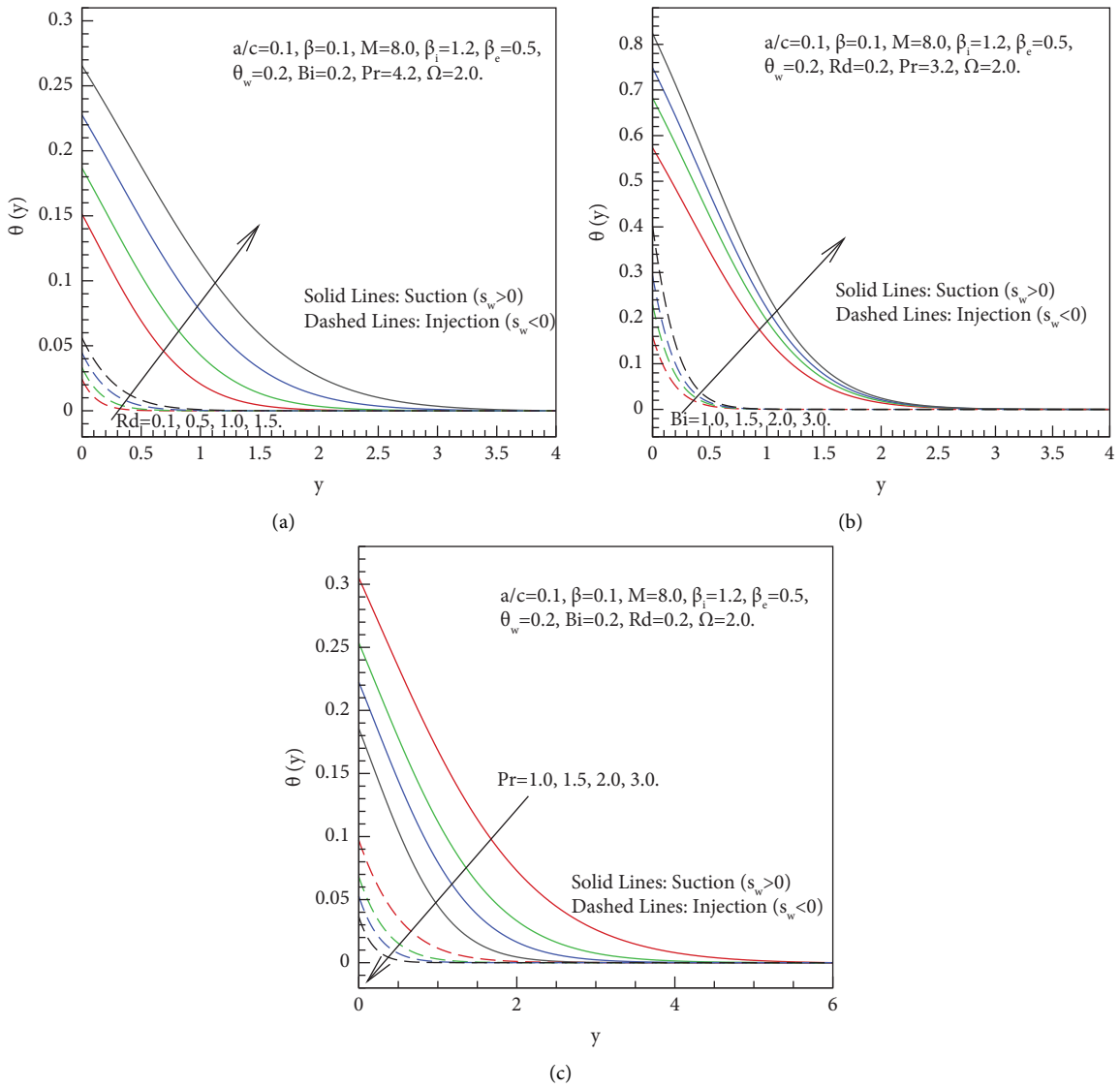

FIGURE 6: (a) Temperature distribution $\theta(y)$ for radiation parameter Rd, (b) temperature distribution $\theta(y)$ for Biot number Bi, and (c) temperature distribution $\theta(y)$ for Prandtl number Pr.

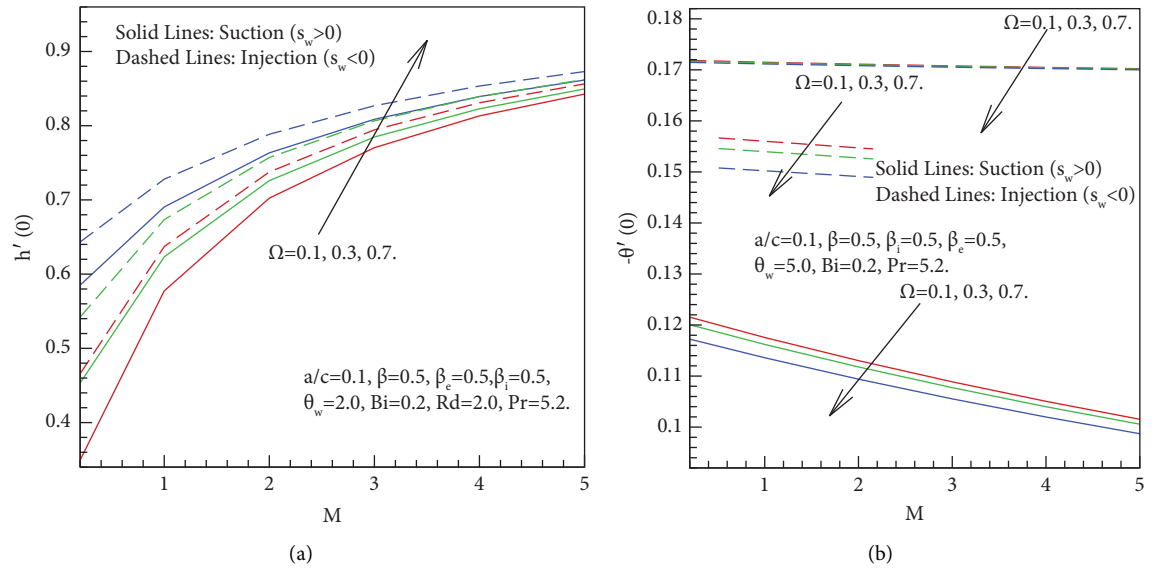

FIGURE 7: (a) Tangential skin friction at surface $-h'(0)$ and (b) heat flux $-\theta'(0)$ for permeability parameter Ω against magnetic field parameter M.

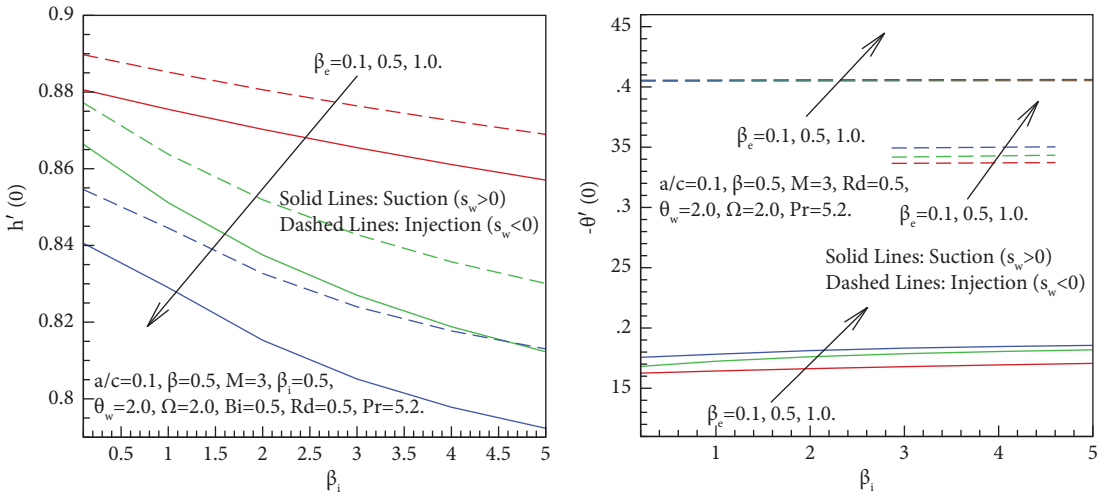

Figure 8: (a) Tangential skin friction at surface $-h^{'}(0)$ and (b) heat flux $-\theta^{'}(0)$ for Hall parameter β_e against ion slip parameter β_i.

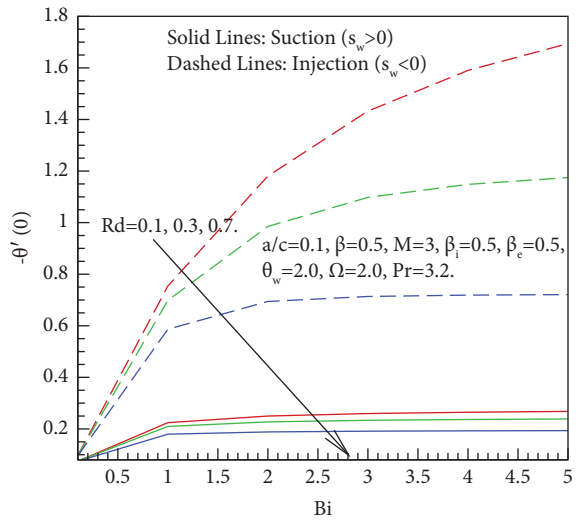

Figure 9: Heat flux $-\theta^{'}(0)$ for radiation parameter Rd against number Bi.

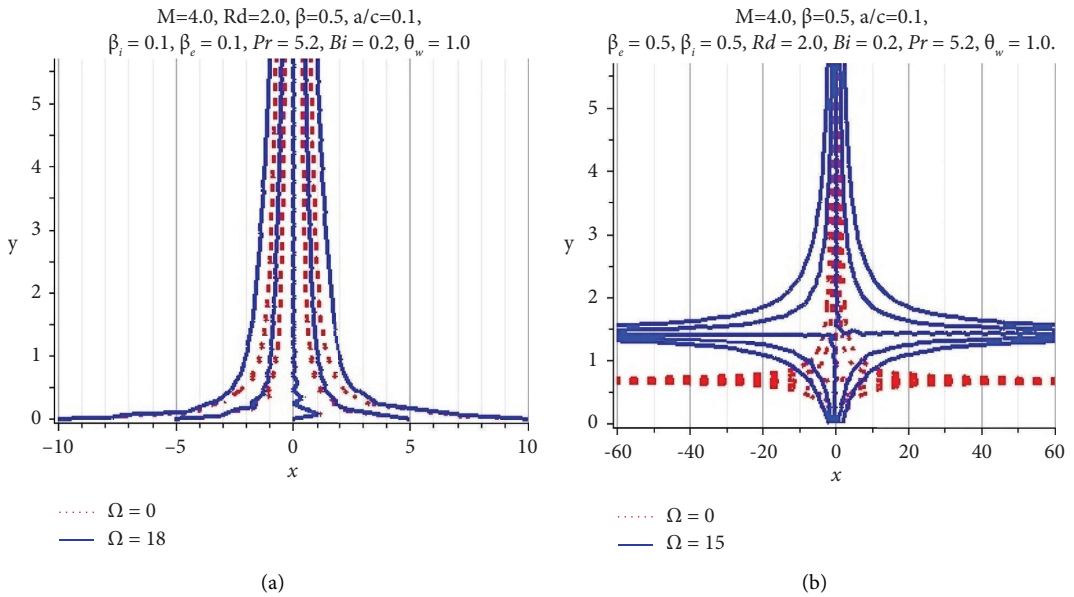

Figure 10: Continued.

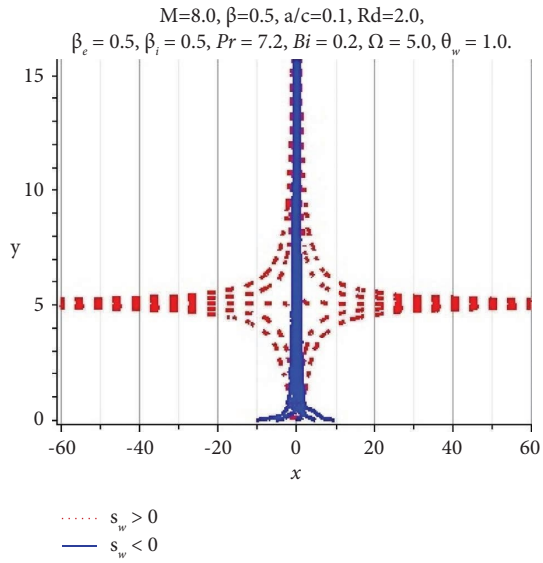

(c)

Figure 10: Stream lines (a) for permeability parameter with injection, (b) for permeability parameter with suction, and (c) for suction and injection.

Table 1: Consequences of local heat flux $-\theta'(0)$ for restrictive case when $Bi \longrightarrow \infty$.

Pr	Existing values	Makinde and Aziz [40]	Khan and Pop [41]	Wang [42]
0.2	0.1696	0.1691	0.1691	0.1691
0.7	0.4541	0.4539	0.4539	0.4539
2.0	0.9113	0.9114	0.9113	0.9113
7.0	1.8950	1.8954	1.8954	1.8954
20.0	3.3533	3.3539	3.3539	3.3539
70.0	6.4620	6.4622	6.4621	6.4621

well as injection ($s_w < 0$). The stream contour ψ touches the partition $y = 0$, at stagnation point x, and zero skin friction.

Table 1 provides the comparison of numerical values of local heat flux with previously published results in literature, so that to authenticate the current computational results. For this purpose, the findings of Makinde and Aziz [40], Khan and Pop [41], and Wang [42] are compared with present values of heat transfer rate in Table 1. Here, the assumptions that are made for comparison are fixed temperature with very large Biot number ($Bi \longrightarrow \infty$) in BCs also with negligence of permeability parameter and suction/injection effects. These values depicted in the table that the current results of heat flux at surface $-\theta'(0)$ against several numerical figures of Prandtl number Pr took upto 3 decimal places with those values of heat flux presented in [40–42].

6. Concluding Remarks

The major presentation of this type of existing research is particularly in the field of aerodynamics and astral, planetary, cosmological, and astrophysical disciplines so that drag may minimize to reduce the loss of energy. So, in this respect, the prevailing article inspects the blend suction injection in permeable surface for non-Newtonian fluid with MHD Hall and ion slip effects over a nonlinear thermally radiative stretched surface. The nonlinear radiative electrically conducting fluid flow in manifestation of magnetic field is widely bump into electrical control generators, cosmological flows, stellar and lunar power control machinery, planetary automobile re-entry, fissionable production plants, and many other engineering areas.

(i) Permeability Ω developed the cause to decline in both velocities but enhances temperature of fluid as this happens in fluids due to high permeability so it allows fluids to pass through more freely. This can be helpful in materials such as aquifers, petroleum reservoirs, cements, and ceramics.

(ii) Ion and Hall slip parameters β_i and β_e are the causes for rise in velocities. Several engineering issues including those involving power generators, magneto hydrodynamic accelerators, refrigeration coils, transmission lines, electric transformers, and heating used these types of currents.

(iii) Velocities for magnetic field parameter M falls down for $M > 1$. But for temperature distribution, it rises. Also, both velocities for magnetic field parameter with suction ($s_w > 0$) is recognized more superior than occurrence of injection ($s_w < 0$). The discovery that the interaction of a plasma with a magnetic field could take place at far greater temperatures than were feasible in a spinning mechanical turbine served as the initial catalyst for interest in MHD power generation.

(iv) Influence of radiation parameter Rd and Biot number Bi on temperature of fluid is more dominant, but for Prandtl number Pr, it became subservient. Several different applications, such as

thermal management, spectroscopy, optoelectronics, and energy-conversion devices, depend on the capacity to control heat radiation.

(v) Local heat flux is enormous for ion and Hall slip parameter β_i and β_e with injection as compared to suction

(vi) Heat transfer rate at surface drops down in the presence of radiation parameter Rd, while it flourishes against different values of Biot number Bi, injection in this case is more prominent than suction. Suction/injection is a mechanical phenomenon that is used to control the fluid flow in the channel and reduce surface drag in order to reduce energy losses in the boundary layer region.

(vii) A solid confirmation is obtained in tabular format of numerical figures with present existing literature. An outstanding agreement is attained for restrictive case.

(viii) A strong convective boundary condition indicated that for numerous figures of Prandtl number, local heat flux at surface upturns

Nomenclature

u:	x–components of velocity
ν:	Viscosity
ρ:	Density
Ω:	Permeability parameter
T_∞:	Free stream temperature
c_p:	Specific heat of fluid
q_r:	Nonlinear radiative heat flux
Rd:	Radiation parameter
β_e:	Hall parameter, ion parameter
β_i:	Hall parameter, ion parameter
$Pr = (\nu/a)$:	Prandtl number
BCs:	Boundary conditions
(b/c):	Obliqueness of fluid flow
ODEs:	Ordinary differential equations
v:	y–components of velocity
p:	Pressure
T:	Temperature
h_s:	Heat transfer coefficient
$a, b.c$:	Constants
k:	Thermal conductivity
$\beta = \mu_B(\sqrt{2\pi_c}/p_y)$:	Casson fluid parameter
$\theta_w = T_f/T_\infty$:	Temperature ratio parameter
$M = (\sigma/c\rho){B_0}^2$:	Magnetic field constraint
s_w:	Suction $(s_w > 0)$/injection $(s_w < 0)$ parameter
(a/c):	Stretching ratio constraint
$Bi = -(h/k)\sqrt{(\nu)}$:	Biot number
A:	Boundary layer displacement constant
PDEs:	Partial differential equations.

Data Availability

No underlying data were collected or produced in this study.

Conflicts of Interest

The authors declare that they have no conflicts of interest with any individual or organization regarding publication of this research.

Acknowledgments

The authors were thankful for technical and financial support from University of Wah, HITEC University, and Shandong University of Science and Technology, Qingdao, China.

References

[1] R. S. Rivlin and J. L. Ericksen, "Stress-deformation relations for isotropic materials," *Collected Papers of RS Rivlin*, pp. 911–1013, Springer-Verlag New York Inc, Newyork, NY, USA, 1997.

[2] W. Noll and C. A. Truesdell, *The Non-linear Field Theories of Mechanics*, Springer-Verlag Berlin, Newyork, NY, USA, 1992.

[3] M. M. Denn, "Fifty years of non-Newtonian fluid dynamics," *AIChE Journal*, vol. 50, no. 10, pp. 2335–2345, 2004.

[4] Y. Lok, N. Amin, and I. Pop, "Non-orthogonal stagnation point flow towards a stretching sheet," *International Journal of Non-linear Mechanics*, vol. 41, no. 4, pp. 622–627, 2006.

[5] F. Labropulu, D. Li, and I. Pop, "Non-orthogonal stagnation-point flow towards a stretching surface in a non-Newtonian fluid with heat transfer," *International Journal of Thermal Sciences*, vol. 49, no. 6, pp. 1042–1050, 2010.

[6] T. R. Mahapatra, S. K. Nandy, and A. S. Gupta, "Oblique stagnation-point flow and heat transfer towards a shrinking sheet with thermal radiation," *Meccanica*, vol. 47, no. 6, pp. 1325–1335, 2012.

[7] M. A. Sadiq, A. U. Khan, S. Saleem, and S. Nadeem, "Numerical simulation of oscillatory oblique stagnation point flow of a magneto micropolar nanofluid," *RSC Advances*, vol. 9, no. 9, pp. 4751–4764, 2019.

[8] R. Tabassum, R. Mehmood, O. Pourmehran, N. Akbar, and M. Gorji-Bandpy, "Impact of viscosity variation on oblique flow of Cu–H2O nanofluid," *Proceedings of the Institution of Mechanical Engineers - Part E: Journal of Process Mechanical Engineering*, vol. 232, no. 5, pp. 622–631, 2018.

[9] M. N. Sadiq, E. Mahmood, M. Sajid, and N. Ali, "Effects of lubrication on the steady oblique stagnation-point flow of a couple stress fluids," *Physics & Astronomy International Journal*, vol. 2, no. 4, pp. 389–397, 2018.

[10] P. Pattnaik, M. M. Bhatti, S. R. Mishra, M. A. Abbas, and O. A. Bég, "Mixed convective-radiative dissipative magnetized micropolar nanofluid flow over a stretching surface in porous media with double stratification and chemical reaction effects: ADM-Padé computation," *Journal of Mathematics*, vol. 2022, Article ID 9888379, 19 pages, 2022.

[11] R. Cortell, "Suction, viscous dissipation and thermal radiation effects on the flow and heat transfer of a power-law fluid past an infinite porous plate," *Chemical Engineering Research and Design*, vol. 89, no. 1, pp. 85–93, 2011.

[12] Z. Uddin and M. Kumar, "Radiation effect on unsteady MHD heat and mass transfer flow on a moving inclined porous heated plate in presence of chemical reaction," *International Journal of Mathematical Modeling, Simulation and Applications*, vol. 3, no. 2, pp. 155–163, 2010.

[13] W. Ibrahim and T. Anbessa, "Three-dimensional MHD mixed convection flow of casson nanofluid with Hall and ion slip effects," *Mathematical Problems in Engineering*, vol. 2020, Article ID 8656147, 15 pages, 2020.

[14] M. V. Krishna, C. Sravanthi, and R. S. R. Gorla, "Hall and ion slip effects on MHD rotating flow of ciliary propulsion of microscopic organism through porous media," *International Communications in Heat and Mass Transfer*, vol. 112, Article ID 104500, 2020.

[15] K. Rajakumar, K. Balamurugan, M. Umasankara Reddy, and C. V. Ramana Murthy, "Radiation, dissipation and Dufour effects on MHD free convection Casson fluid flow through a vertical oscillatory porous plate with ion-slip current," *International Journal of Heat and Technology*, vol. 36, no. 2, pp. 494–508, 2018.

[16] S. J. Kumar and S. Vishwanath, "Hall and ion-slip effects on MHD free convective flow of a viscoelastic fluid through porous regime in an inclined channel with moving magnetic field," *Kragujevac Journal of Science*, vol. 42, pp. 5–18, 2020.

[17] Z. Shah, S. Islam, H. Ayaz, and S. Khan, "Radiative heat and mass transfer analysis of micropolar nanofluid flow of Casson fluid between two rotating parallel plates with effects of Hall current," *Journal of Heat Transfer*, vol. 141, no. 2, 2019.

[18] K. Ramesh and O. Ojjela, "Entropy generation analysis of natural convective chemically reacting squeezing flow of Casson fluid between parallel disks with Hall and Ion slip currents," *Heat Transfer - Asian Research*, vol. 48, no. 8, pp. 4320–4341, 2019.

[19] C. RamReddy, O. Surender, and C. V. Rao, "Effects of Soret, Hall and Ion-slip on mixed convection in an electrically conducting Casson fluid in a vertical channel," *Nonlinear Engineering*, vol. 5, no. 3, pp. 167–175, 2016.

[20] R. Vijayaragavan and S. Karthikeyan, "Hall current effect on chemically reacting MHD Casson fluid flow with dufour effect and thermal radiation," *Asian J Appl Sci Technol*, vol. 2, no. 2, pp. 228–245, 2018.

[21] M. Abd El-Aziz and A. S. Yahya, "Perturbation analysis of unsteady boundary layer slip flow and heat transfer of Casson fluid past a vertical permeable plate with Hall current," *Applied Mathematics and Computation*, vol. 307, pp. 146–164, 2017.

[22] W. Ibrahim and T. Anbessa, "Mixed convection flow of nanofluid with Hall and ion-slip effects using spectral relaxation method," *Journal of the Egyptian Mathematical Society*, vol. 27, no. 1, pp. 52–21, 2019.

[23] M. Shojaefard, "Numerical investigation of flow control by suction and injection on a subsonic airfoil," *American Journal of Applied Sciences*, vol. 2, no. 10, 2005.

[24] A. Braslow, *History of Suction-type Laminar-Flow Control with Emphasis on Flight Resrearch: Monographs in Aerospace History*, NASA History, Washington, DC, USA, 1999.

[25] A. Zeeshan and A. Majeed, "Heat transfer analysis of Jeffery fluid flow over a stretching sheet with suction/injection and magnetic dipole effect," *Alexandria Engineering Journal*, vol. 55, no. 3, pp. 2171–2181, 2016.

[26] H. A. El-Arabawy, "Effect of suction/injection on the flow of a micropolar fluid past a continuously moving plate in the presence of radiation," *International Journal of Heat and Mass Transfer*, vol. 46, no. 8, pp. 1471–1477, 2003.

[27] A. Chamkha, A. Aly, and M. Mansour, "Similarity solution for unsteady heat and mass transfer from a stretching surface embedded in a porous medium with suction/injection and chemical reaction effects," *Chemical Engineering Communications*, vol. 197, no. 6, pp. 846–858, 2010.

[28] A. K. Pandey and M. Kumar, "Effect of viscous dissipation and suction/injection on MHD nanofluid flow over a wedge with porous medium and slip," *Alexandria Engineering Journal*, vol. 55, no. 4, pp. 3115–3123, 2016.

[29] L. Rundora and O. Makinde, "Effects of suction/injection on unsteady reactive variable viscosity non-Newtonian fluid flow in a channel filled with porous medium and convective boundary conditions," *Journal of Petroleum Science and Engineering*, vol. 108, pp. 328–335, 2013.

[30] N. A. Haroun, P. Sibanda, S. Mondal, and S. S. Motsa, "On unsteady MHD mixed convection in a nanofluid due to a stretching/shrinking surface with suction/injection using the spectral relaxation method," *Boundary Value Problems*, vol. 2015, no. 1, p. 24, 2015.

[31] S. Hamrelaine, F. Mebarek-Oudina, and M. R. Sari, "Analysis of MHD Jeffery Hamel flow with suction/injection by homotopy analysis method," *J. Adv. Res. Fluid Mech. Therm. Sci*, vol. 58, no. 2, pp. 173–186, 2019.

[32] M. Ganapathirao, R. Ravindran, and I. Pop, "Non-uniform slot suction (injection) on an unsteady mixed convection flow over a wedge with chemical reaction and heat generation or absorption," *International Journal of Heat and Mass Transfer*, vol. 67, pp. 1054–1061, 2013.

[33] R. Tabassum and R. Mehmood, "Crosswise stream of methanol–iron oxide (CH3OH–Fe3O4) with temperature-dependent viscosity and suction/injection effects," *Proceedings of the Institution of Mechanical Engineers - Part E: Journal of Process Mechanical Engineering*, vol. 233, no. 5, pp. 1013–1023, 2019.

[34] S. Abo-Dahab, M. A. Abdelhafez, F. Mebarek-Oudina, and S. M. Bilal, "MHD casson nanofluid flow over nonlinearly heated porous medium in presence of extending surface effect with suction/injection," *Indian Journal of Physics*, vol. 95, no. 12, pp. 2703–2717, 2021.

[35] A. K. Pandey and M. Kumar, "Squeezing unsteady MHD Cu–water nanofluid flow between two parallel plates in porous medium with suction/injection," *Computational and Applied Mathematics Journal*, vol. 4, no. 2, pp. 31–42, 2018.

[36] B. K. Jha, B. Aina, and S. Muhammad, "Combined effects of suction/injection and wall surface curvature on natural convection flow in a vertical micro-porous annulus," *Thermophysics and Aeromechanics*, vol. 22, no. 2, pp. 217–228, 2015.

[37] S. Rana, R. Mehmood, and N. S. Akbar, "Mixed convective oblique flow of a Casson fluid with partial slip, internal heating and homogeneous–heterogeneous reactions," *Journal of Molecular Liquids*, vol. 222, pp. 1010–1019, 2016.

[38] R. Mehmood, S. Rana, N. Akbar, and S. Nadeem, "Non-aligned stagnation point flow of radiating Casson fluid over a stretching surface," *Alexandria Engineering Journal*, vol. 57, no. 2, pp. 939–946, 2018.

[39] K. Mahmud, S. Rana, A. Al-Zubaidi, R. Mehmood, and S. Saleem, "Interaction of Lorentz force with cross swimming microbes in couple stress nano fluid past a porous Riga plate,"

International Communications in Heat and Mass Transfer, vol. 138, Article ID 106347, 2022.

[40] O. D. Makinde and A. Aziz, "Boundary layer flow of a nanofluid past a stretching sheet with a convective boundary condition," *International Journal of Thermal Sciences*, vol. 50, no. 7, pp. 1326–1332, 2011.

[41] W. Khan and I. Pop, "Boundary-layer flow of a nanofluid past a stretching sheet," *International Journal of Heat and Mass Transfer*, vol. 53, no. 11-12, pp. 2477–2483, 2010.

[42] C. Wang, "Free convection on a vertical stretching surface," *ZAMM-Journal of Applied Mathematics and Mechanics/ Zeitschrift für Angewandte Mathematik und Mechanik*, vol. 69, no. 11, pp. 418–420, 1989.